Calcification-driven CO2 emissions exceed “Blue Carbon” sequestration in a carbonate seagrass meadow

Bryce Van Dam (vandam.bryce@gmail.com)
Helmholtz-Zentrum Geesthacht https://orcid.org/0000-0003-0876-1392
Mary Zeller
Leibniz Institute for Baltic Sea Research https://orcid.org/0000-0001-6952-4273
Christian Lopes
Florida International University
Ashley Smyth
University of Florida
Michael Böttcher
Leibniz Institute for Baltic Sea Research
Christopher Osburn
North Carolina State University https://orcid.org/0000-0002-9334-4202
Tristan Zimmerman
Helmholtz-Zentrum Geesthacht
Daniel Pröfrock
Helmholtz-Zentrum Geesthacht
James Fourqurean
Florida International University
Helmuth Thomas
Helmholtz-Center Geesthacht, Institute for Coastal Research

Physical Sciences - Article

Keywords: Alkalinity Exchanges, Denitrification, Inorganic Carbon Cycling, Eddy Covariance, Ecosystem Calcification, Climate Change Mitigation

Posted Date: January 14th, 2021

DOI: https://doi.org/10.21203/rs.3.rs-120551/v1

Calcification-driven CO_2 emissions exceed "Blue Carbon" sequestration in a carbonate seagrass meadow

[1]Bryce R Van Dam, [2]Mary A Zeller, [3]Christian Lopes, [4]Ashley R Smyth, [2]Michael E. Böttcher, [5]Christopher L Osburn, [1]Tristan Zimmerman, [1]Daniel Pröfrock, [3]James W Fourqurean, [1]Helmuth Thomas

[1]Institute of Coastal Research, Helmholtz-Zentrum Geesthacht, Geesthacht, Germany. [2]Geochemistry and Isotope BioGeoChemistry Group, Department of Marine Geology, Leibniz Institute for Baltic Sea Research, Warnemünde, Germany. [3]Institute of Environment, Department of Biological Sciences, Florida International University, Miami, Florida, USA. [4]Soil and Water Sciences Department, Tropical Research and Education Center, University of Florida, Homestead, Florida, USA. [5]Department of Marine, Earth and Atmospheric Sciences, North Carolina State University, Raleigh, North Carolina, USA

Abstract

Long-term "blue carbon" burial in seagrass meadows is complicated by other carbon and alkalinity exchanges that shape net carbon sequestration. We measured a suite of such processes, including denitrification, sulfur, and inorganic carbon cycling, and assessed their impact on air-water carbon dioxide exchange in a typical seagrass meadow underlain by carbonate sediments. Contrary to the prevailing concept of seagrass meadows acting as carbon sinks, eddy covariance measurements reveal this ecosystem as a consistent source of carbon dioxide to the atmosphere, at an average rate of 610 ± 990 µmol m^{-2} hr^{-1} during our study and 700 ± 660 µmol m^{-2} hr^{-1}over an annual cycle. A robust mass-balance shows that net alkalinity consumption by ecosystem calcification explains >95% of the observed carbon dioxide emissions, far exceeding alkalinity generated by net reduced sulfur, iron and organic carbon burial. Isotope geochemistry of porewaters suggests substantial dissolution and re-crystallization of more stable carbonates mediated by sulfide oxidation-induced acidification, enhancing long-term carbonate burial and ultimate carbon dioxide production. We show that the "blue carbon" sequestration potential of calcifying seagrass meadows has been over-estimated, and that *in-situ* organic carbon burial only offsets a small fraction (<5%) of calcification-induced CO_2 emissions. Ocean-based climate change mitigation activities in such calcifying regions should be approached with caution and an understanding that net carbon sequestration may not be possible.

Main

Seagrass ecosystems are some of the most organic carbon-dense systems on earth, and it has been argued that organic carbon sequestration here is disproportionately large in comparison with other terrestrial and marine ecosystems, thus constituting an important sink in the global carbon cycle[1,2]. Presently, there exists a nearly dogmatic consensus that the protection and enhancement of such "Blue Carbon" storage in seagrass meadows is an effective strategy to mitigate increasing atmospheric CO_2 levels[3-7]. However, biogeochemical cycling in seagrass ecosystems is complex, and many other processes exist which may counteract net organic carbon sequestration. These processes collectively regulate local budgets of dissolved inorganic carbon (DIC) and total alkalinity (TA), including ecosystem calcification[8-10] and anaerobic metabolism[11]. When net TA production occurs, the resulting carbonate system re-equilibration consumes CO_2 which is then compensated by net CO_2 uptake from the atmosphere. The ultimate impact of these TA-generating processes (namely iron (Fe), sulfate (SO_4^{2-}), and nitrate (NO_3^-) reduction), on net CO_2 uptake depends on whether the metabolic products are permanently removed or if they are re-oxidized. Competing with these TA sources, a key sink for TA (source of CO_2) in Blue Carbon habitats is the precipitation of carbonate minerals[5,12,13]. This is especially so in tropical and subtropical seagrasses, which play a disproportionately large role in the global carbonate cycle[14]. The impact of these internal re-workings of S, Fe, N, and carbonate minerals on surface water TA/DIC, and ultimately air-sea CO_2 exchange remains largely unknown. This has been identified as a key gap in our understanding of the role of Blue Carbon ecosystems in the global carbon cycle[10,15].

Despite the understanding that carbonate precipitation generates CO_2, carbonate seagrass meadows are still considered as important Blue Carbon sinks based largely on the assumption that these carbonate minerals were formed elsewhere[10,12], or that the CO_2 produced by calcification is rapidly consumed by photosynthesis[16]. As a result, policies aimed at restoring or protecting Blue Carbon habitats have gathered momentum as an approach to fight climate change, while also achieving co-benefits of habitat improvement[4,5,17]. In recent IPCC reports, these ocean-based mitigation tools have been assigned a high chance of success[18] (IPCC Chapter 5.5.1.2.2), despite the lack of empirical evidence demonstrating net CO_2 uptake by carbonate seagrass meadows[13]. Still, uncertainty in the scientific community regarding the role of calcification in Blue Carbon mitigation is explicitly acknowledged by the IPCC, and its timely resolution is seen as "highly desirable"[18]. Blue Carbon mitigation requires public and private buy-in[4,19], and a general understanding that the actions taken will indeed enhance net carbon sequestration. Many of these Blue Carbon habitats are managed by resource-limited nations, introducing a climate injustice risk, as there exists a perception that they are being asked to carry the climate burden of more industrialized nations[20]. It is

therefore crucial that these ocean-based management actions only be enacted for Blue Carbon habitats where increased carbon sequestration is plausible.

To address these uncertainties, we used atmospheric eddy covariance (EC) to directly measure air-water CO_2 exchange in Florida Bay, USA, one of the largest seagrass-dominated estuaries in the world, and a known organic carbon sink[21]. We combine these EC fluxes with geochemical approaches to attribute the major processes contributing to source or sink behavior. We sampled at 3 locations in close proximity within this seagrass meadow, representing regions of 1) high seagrass aboveground biomass (HD), 2) low seagrass density (LD), and 3) bare sediment (B). We combined pore-water and solid-phase analysis with a continuous-flow incubation that either included or excluded living seagrass biomass. This approach lets us ascribe changes in surface water TA and DIC to net process rates in the sediment, which were in turn integrated into a biogeochemical budget, assessing their effects on air-water CO_2 uptake or release.

Net CO_2 emissions associated with carbonate mineral dissolution/re-precipitation

Direct EC measurements reveal this seagrass meadow as a moderate source of CO_2 to the atmosphere (Figure 1B,C), with average emissions during the ~one-week study period of 610 ± 990 µmol m^{-2} hr^{-1} (green line in Figure 1C; mean ± 1 SD of 30-min records). This is slightly below the previously-reported summer-time CO_2 flux for this site[22] (972 ± 612 µmol m^{-2} hr^{-1}), and just below the annual average (black line in Figure 1C; 700 ± 660 µmol m^{-2} hr^{-1}). While annual hourly climatology demonstrates a clear diel trend, with greater CO_2 emissions during the afternoon (Figure 1B), such a day-night difference was not present during the study period (Wilcoxon, $p = 0.61$). This is consistent with the hypothesis that factors other than seagrass net ecosystem metabolism control the CO_2 system at this site, contrasting with prior studies describing the importance of water-column productivity for seasonal CO_2 uptake in the fall[23,24]. These CO_2 emissions constitute a basement assessment of the global warming potential of this seagrass meadow, which is likely enhanced by the release of other greenhouse gases[25] like methane and N_2O.

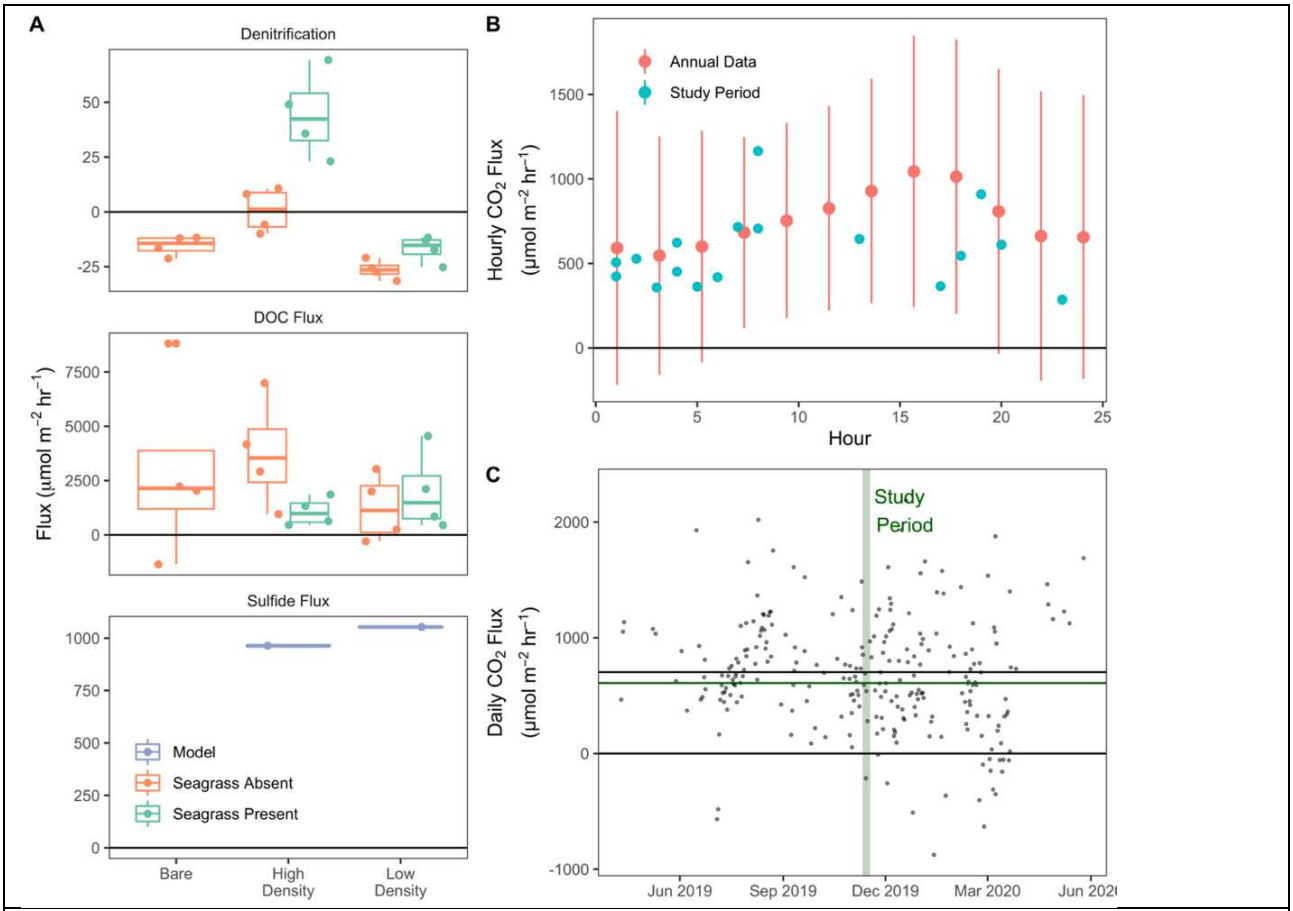

Figure 1. Boxplots showing average N_2 flux (denitrification), DOC fluxes, and sulfide fluxes (A). Hourly and daily climatological mean CO_2 fluxes, from direct EC measurements in the year surrounding the study period (B,C). In (C), the timeframe of the study period is highlighted in green, while mean CO_2 fluxes from the study period and annually are shown as the green and black horizontal lines, respectively. By convention, release from sediments or water are reported as positive fluxes. All error bars represent $\bar{x}$ ± standard deviation.

In line with strong carbonate dissolution, we observed significant excesses of pore-water DIC coinciding with a moderate (Low-density seagrass site "LD") or large (High-density seagrass, "HD") enrichment of ^{13}C in DIC, such that average pore-water $\delta^{13}C_{DIC}$ (-1.7 ± 1.4‰) was at least 2‰ 'heavier' than surface water ($\delta^{13}C_{DIC}$ = -3.9 ± 0.02‰) (Figure 2). For sediment depths outside of the zone of peak DIC accumulation, a Keeling plot points towards an isotopic endmember of ~0‰, characteristic of 'heavy' DIC from carbonate mineral dissolution mixed with 'light' respiratory DIC from organic carbon degradation ($\delta^{13}C_{DOC}$ = -18 ± 1.9‰). However, within the DIC maximum zone in the HD cores, DIC was significantly enriched in ^{13}C with an average $\delta^{13}C_{DIC}$ of 0.0 ± 1.1‰ (-2.1 ± 0.6‰ in the LD cores). The isotopic endmember indicated for this "DIC-maximum zone" is well above measured $\delta^{13}C_{PIC}$ of 1.9 ± 0.12‰. Enrichment in ^{13}C of this magnitude cannot be explained solely by $CaCO_3$ dissolution. Rather, this enrichment necessitates the consumption of isotopically light pore-water DIC by carbonate precipitation, under quasi closed-system conditions[26]. This hypothesis is supported by the modeled DIC production rates (Figure 2F), where net DIC generated below 10 cm depth is consumed in the upper 10 cm of sediment by combined autotrophic sulfide oxidation and carbonate re-precipitation. Likewise, decreased solid-phase Ca:Sr and Ca:Mg ratios in the upper 10-20 cm of sediment support carbonate mineral recrystallization in this region (Figure 3 C,D). Our findings are consistent with prior work showing this coupled dissolution/re-precipitation to be highest when seagrasses are especially dense[26,27]. This internal carbonate recycling is critically important to the overall C cycle, as it regulates the burial efficiency of $CaCO_3$, ultimately governing CO_2 emissions related to net carbonate burial.

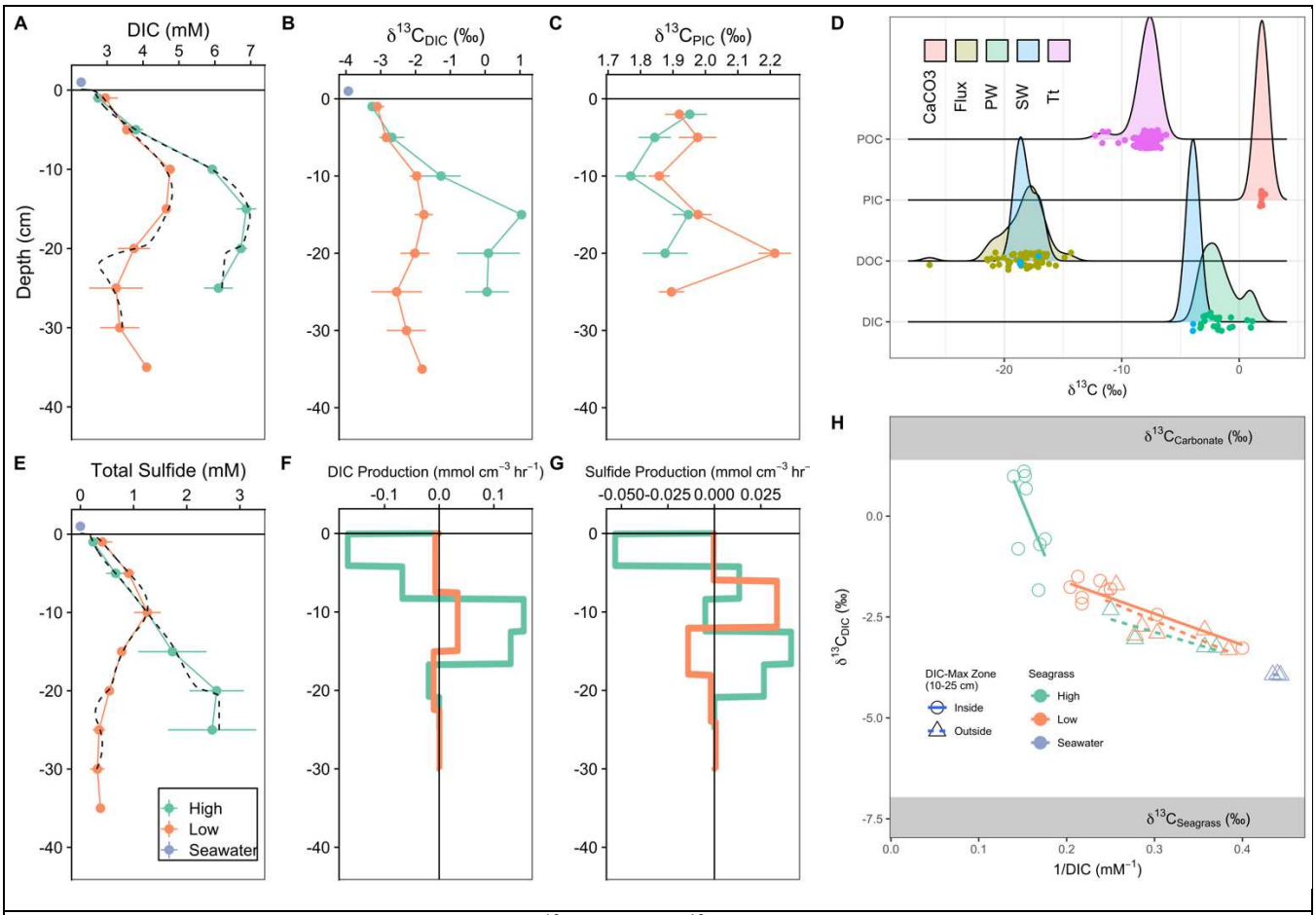

Figure 2. Vertical profiles of pore-water DIC, $\delta^{13}C_{DIC}$, and $\delta^{13}C_{PIC}$ (A-C). Carbon isotopic signatures for selected pools (D). Total dissolved sulfide (E), and modeled production rates for DIC and total Sulfide (F, G). 'Keeling Plot' of pore-water $\delta^{13}C_{DIC}$ (H). Model output pore-water concentrations are shown in the black dotted lines in figures A-B (each core was modeled individually).

Denitrification and sulfate reduction are only minor alkalinity sources

Pore-water total dissolved sulfide was significantly elevated relative to surface water (Figure 2E), especially in the HD cores, and was generated by net sulfate reduction at depths of ~10 (LD) to ~15 (HD) cm (Figure 2G). This excess sulfide corresponded to a large modeled vertical sulfide flux (Figure 1A) that was presumably re-oxidized in the narrow oxic zone of the sediments or the water column. All dissolved sulfide samples from the sediment flux incubation were below the limit of detection, confirming that reduced sulfur

diffusing upwards is quantitatively lost to either 1) oxidation to sulfate, or 2) burial as $FeS_2 + S^0$ (Figure 3A), or 3) burial as FeS. We expect that sulfide oxidation is largely limited to depths of 0-30 cm, as the relative increase in Mo (a redox-sensitive tracer) below 30 cm depth (Figure 3B) indicate permanent anoxia below this threshold. While bulk sediments of the upper 0-30 cm are also anoxic, the relative Mo depletion in this zone supports localized and sporadic oxidation in the millimeters surrounding seagrass roots. The impact of net sulfate reduction on TA depends on the fate and form of net reduced sulfur burial. To this point, we observe significant accumulation of Chromium (II) Reducible Sulfur (CRS; $FeS_2 + S^0$), with an average content of 94 ± 37 µmol CRS g^{-1} (0.3 ± 0.12 % dry weight), and a peak of 200 µmol g^{-1} in the peak sulfate reduction zone of site HD. Lower concentrations of AVS (maximum of 3.6, average of 2.4 ± 1.8 µmol g^{-1}) indicates a relatively minor contribution of H_2S and FeS to total sulfur burial. Because the total Fe content (44.9 ± 5.3 µmol g^{-1}) is half of average CRS, at most ~100% of reduced sulfur may be buried as pyrite (FeS_2). However, prior work[28] shows that 50% or more of the sedimentary Fe pool in central Florida Bay is not directly associated with CRS, suggesting substantial burial of elemental sulfur (S^0) as a product of partial sulfide re-oxidation[29]. This is supported by the CRS peak at 10 cm at the HD site, possibly caused by sulfide oxidation to sulfur at the surface of seagrass roots[30]. Assuming CRS is composed of equal proportions FeS_2 and S^0, net sulfate reduction and burial will produce TA and DIC in a ratio of 2:1 (Table 1).

Continuous-flow incubations conducted in the dark showed that denitrification was closely balanced by N fixation, and only cores from the HD site with seagrass biomass included were on average net denitrifying (positive N_2 flux). In contrast, all other cores were net N fixing, despite dark conditions favorable to net denitrification[31] (Figure 1A). Averaged across all cores, net denitrification was not significantly different from zero ($\bar{x}$ = -3 ± 27 µmol m^{-2} hr^{-1}), consistent with the understanding that denitrification in seagrass meadows is spatially heterogeneous, tends to co-vary with autochthonous organic matter input[32,33], and is part of a highly conservative N cycle. Our low denitrification measurements are also consistent with the low nitrate concentrations typical of many carbonate seagrasses[34], where all available nitrate appears to be quantitatively denitrified. That net denitrification was only observed in cores from the HD site containing living seagrass biomass (Figure 1A), where pore-water sulfide was also maximized (Figure 2E), contrasts with the expected sulfide inhibition of denitrification in Florida Bay[33]. Instead, denitrification may have been enhanced by the leaching of labile OM leaching from the seagrass rhizosphere. Likewise, the dissolution of carbonate sediments, as expected during this dark/heterotrophic incubation, is a potential abiotic source of dissolved OM through the release of carbonate-associated organic matter[35]. We posit these abiotic and biotic OM sources together drove our large measured DOC fluxes. Broadly, the observation of strong internal recycling with respect to N and S supports

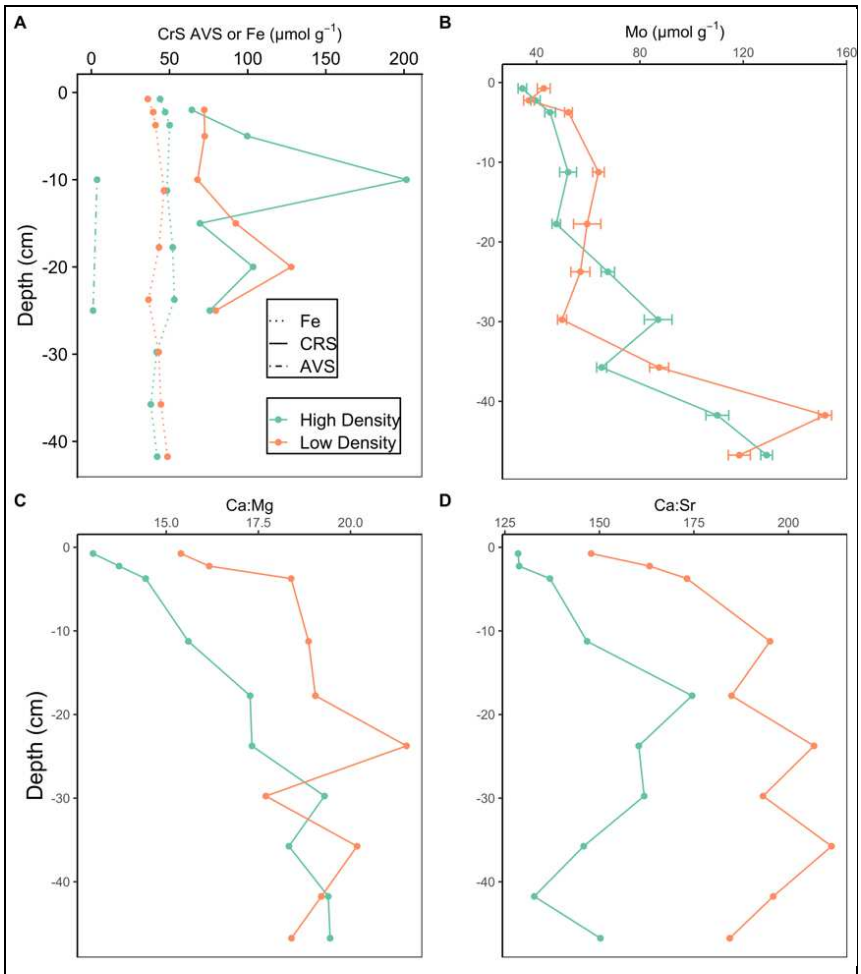

Figure 3. Solid-phase total Fe, Chromium Reducible Sulfur (CRS) and acid-volatile sulfide (AVS) (A), total Mo (B), and molar ratios of Ca:Mg and Ca:Sr (C,D).

the notion that alkalinity dynamics in this carbonate seagrass meadow is dominated by $CaCO_3$ precipitation and dissolution, rather than anaerobic alkalinity generation via nitrate, sulfate, or metal reduction.

CO_2 emissions are driven by net $CaCO_3$ production

We detected consistent net CO_2 emissions from this seagrass meadow of 610 µmol m^{-2} hr^{-1} over the study period, and 703 µmol m^{-2} hr^{-1} as an annual average (Figure 1B). This is notable given the dogmatic understanding of seagrasses as net Blue Carbon sinks, and in light of our understanding of these seagrasses as being net autotrophic[36]. That CO_2 emissions persisted at this site, despite seagrass ecosystem productivity and known net organic carbon burial[21], suggests that processes besides seagrass net metabolism drive air-water CO_2 exchanges. To find the dominant carbon source for these CO_2 emissions, we constructed a simple TA and DIC budget, considering the impact of calcification (IC accumulation), Fe and SO_4^{2-} reduction (CRS), and net organic carbon (OC) burial. Measured denitrification was not significantly different from 0, hence was excluded as a putative TA source. We found that modeled Excess CO_2 was most sensitive to IC accumulation, which caused 95.8% of the change in Excess CO_2 (Figure 4). CO_2 consumption by net organic carbon accumulation reduced Excess CO_2 by 3.4%, while the burial of CRS and Fe (i.e. net SO_4^{2-} and Fe reduction) only reduced Excess CO_2 by ~1%. When these TA/DIC consuming and producing processes are summed, we find that total Excess CO_2 available for release to the atmosphere (solid black line in Figure 4) increases with sediment accumulation. Using an average gas transfer velocity of 11.7 cm hr^{-1}, our measured CO_2 fluxes can be converted to excess CO_2 values of between 6.0 and 5.2 µmol kg^{-1} (grey dashed lines in Figure 4), well within the range of total Excess CO_2 in the budget. Furthermore, the SAR required to sustain measured annual average CO_2 emissions (700 ± 660 µmol m^{-2} hr^{-1}) is only 460 g sediment m^{-2} yr^{-1} (vertical dotted line in Figure 4), intermediate of literature values for central Florida Bay[37,38].

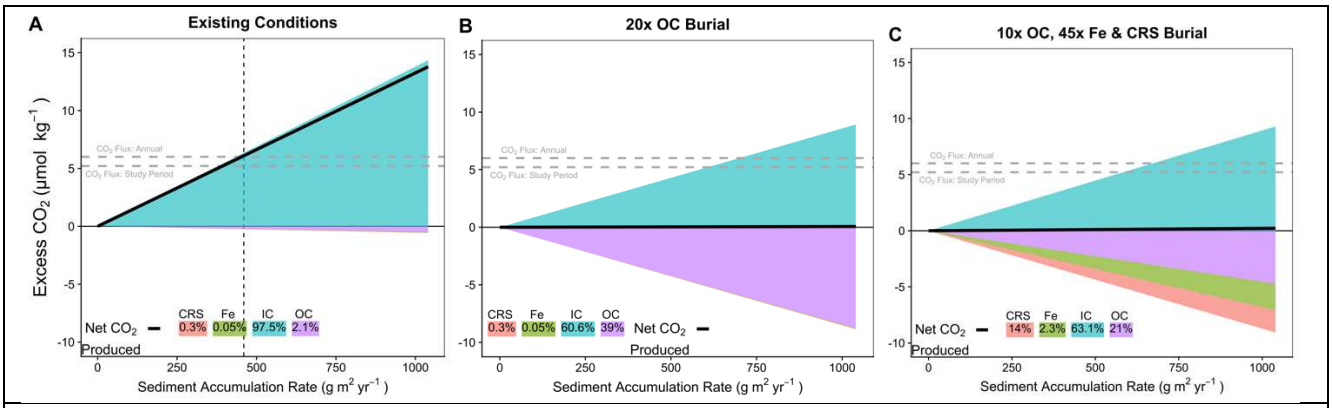

Figure 4. Modeled Excess CO_2, across a range in literature sediment accumulation rates. The bottom subplot is a magnification of the terms constituting net CO_2 uptake (burial of OC, reduced S and Fe). In figure (A) sediment fractions of CRS, Fe, IC, and OC were set according to direct measurements from this study. In figure (B), the OC fraction was artificially increased until Excess CO_2 remained at 0 across the range in sediment accumulation, such that CO_2 released by calcification was offset by CO_2 consumed by OC burial, Fe and SO_4 reduction. In figure (C), net CO_2 balance was achieved by increasing OC, Fe, and CRS fractions by factors of 10, 45, and 45, respectively.

To find the rate of OC burial required to balance the CO_2 produced by calcification, we repeatedly ran the model, increasing the fraction of sediment composed of OC until total Excess CO_2 was equal to 0. For these processes to balance out, the sediment OC fraction would need to increase by a factor of nearly 20, from 2.1% to 39% (compensated by IC decrease from 97.5 to 60.6%; Figure 4B). OC contents of this order are much greater than can be found in carbonate seagrass meadows elsewhere in Florida Bay[39] or globally[40,41]. In a final model, we increased OC burial by only one order of magnitude (to 21%), but increased CRS and Fe fractions by a factor of 45, simulating an artificial Fe amendment scenario. In this admittedly unrealistic scenario, CO_2 emissions due to calcification are balanced approximately equally by OC burial, and anaerobic TA generation by net sulfate and Fe reduction. In these additional scenarios (Figure 4B,C), some unknown additional CO_2 source would be required in order to bring modeled excess CO_2 (thick black line) in line with the excess CO_2 associated with measured CO_2 emissions (grey dashed lines). As nearly one third of seagrass meadows[12] overly sediments with $CaCO_3$ contents exceeding 80% dwt, it is likely that our observation of calcification-driven CO_2 emissions from this seagrass meadow is representative of a significant fraction of carbonate systems globally.

Progress towards realistic "Blue Carbon" accounting

Prior Blue Carbon syntheses have suggested carbonate seagrass meadows as strong carbon sinks, based largely on the assumption that much of the $CaCO_3$ was allochthonous[10,12]. The present study site in central Florida Bay is isolated from coral reefs and other calcifying ecosystems, meaning that all of the $CaCO_3$ buried here is produced in-situ. Measured rates of lime mud production in Florida Bay suggest Florida Bay exports carbonates rather than importing them[42]. Additionally, extensive mud banks throughout Florida Bay restrict horizontal exchange[43], further decreasing the chance of internal $CaCO_3$ re-distribution, as previously suggested[12]. Therefore, our direct EC measurements which reveal net annual emissions of 703 ± 656 µmol CO_2 m^{-2} hr^{-1} (~6 mol m^{-2} yr^{-1}) places this seagrass meadow as a clear net CO_2 source to the atmosphere. Calcification explained essentially all of the measured CO_2 emissions, and exceeded the OC sink by over 300%, rather than offsetting 30-40% of OC burial as prior work indicated[12]. This net $CaCO_3$ burial is sustained by carbonate dissolution and re-precipitation, enhancing $CaCO_3$ burial efficiency and ultimately shaping CO_2 emissions. While OC burial does offset a small fraction (3.4%) of these emissions, an unrealistic 20-fold increase would be required for the site to become a net CO_2 sink. The impact of TA production by net sulfate and Fe reduction is even smaller, offsetting ~1% of the calcification CO_2 emissions.

Our novel comprehensive approach, supported by micro-meteorological and isotope geochemical tools, contributes to the first fundamental evidence towards resolving one of the key uncertainties in Blue Carbon accounting[18,13]. This approach has the potential to serve as a blueprint for future studies in search of coastal ecosystems capable of net atmospheric CO_2 sequestration. As more than a quarter of all Blue Carbon habitats also have high carbonate contents[12] (> 80% dwt), reliable carbon balancing such as this study will help to identify cases of 'surprise' CO_2 emissions[44]. Our study motivates a more rigorous (re-)assessment of the coastal carbon balance, which is essential to protect public and private sectors' initiatives and investments in ocean-based mitigation of climate change as an accountable contribution to the COP21 Paris agreement.

References

1. Fourqurean, J.W., C.M. Duarte, H. Kennedy, N. Marba, M. Holmer, M.A. Mateo, E.T. Apostolaki, G.A. Kendrick, D. Krause-Jensen, K.J. McGlathery, and O. Serrano. 2012a. Seagrass ecosystems as a globally significant carbon stock. Nature Geoscience 5: 505-509.
2. Tokoro, T., Watanabe, K., Tada, K., and Kuwae, T. (2019). "Air–Water CO_2 Flux in Shallow Coastal Waters: Theory, Methods, and Empirical Studies," in *Blue Carbon in Shallow Coastal Ecosystems: Carbon Dynamics, Policy, and Implementation*, eds T. Kuwae and M. Hori, Singapore: Springer. https://doi.org/10.1007/978-981-13-1295-3
3. Duarte, C. M., J. J. Middelburg, and N. Caraco. 2005. Major role of marine vegetation on the oceanic carbon cycle. Biogeosciences 2: 1–8. doi:10.5194/bg-2-1-2005
4. Gattuso, J. P., A. K. Magnan, L. Bopp, and others. 2018. Ocean solutions to address climate change and its effects on marine ecosystems. Front. Mar. Sci. 5. doi:10.3389/fmars.2018.00337
5. Howard, J., A. Sutton-Grier, D. Herr, J. Kleypas, E. Landis, E. Mcleod, E. Pidgeon, and S. Simpson. 2017. Clarifying the role of coastal and marine systems in climate mitigation. Front. Ecol. Environ. 15: 42–50. doi:10.1002/fee.1451
6. Kennedy, H., J. Beggins, C. M. Duarte, J. W. Fourqurean, M. Holmer, N. Marbá, and J. J. Middelburg. 2010. Seagrass sediments as a global carbon sink: Isotopic constraints. Global Biogeochem. Cycles 24: 1–8. doi:10.1029/2010GB003848
7. Needelman, B. A., I. M. Emmer, S. Emmett-Mattox, S. Crooks, J. P. Megonigal, D. Myers, M. P. J. Oreska, and K. McGlathery. 2018. The Science and Policy of the Verified Carbon Standard Methodology for Tidal Wetland and Seagrass Restoration. Estuaries and Coasts 41: 2159–2171. doi:10.1007/s12237-018-0429-0
8. Howard, J. L., J. C. Creed, M. V. P. Aguiar, and J. W. Fouqurean. 2018. CO2 released by carbonate sediment production in some coastal areas may offset the benefits of seagrass "Blue Carbon" storage. Limnol. Oceanogr. 63: 160–172. doi:10.1002/lno.10621
9. Macreadie, P.I., O. Serrano, D.T. Maher, C.M. Duarte, and J. Beardall. 2017. Addressing calcium carbonate cycling in blue carbon accounting. Limnology and Oceanography Letters 2: 195-201.
10. Mazarrasa, I., Marbà, N., Lovelock, C. E., Serrano, O., Lavery, P. S., Fourqurean, J. W., et al. (2015). Seagrass meadows as a globally significant carbonate reservoir. Biogeosciences, 12(16), 4993–5003. https://doi.org/10.5194/bg-12-4993-2015
11. Hu, X., and W. J. Cai. 2011. An assessment of ocean margin anaerobic processes on oceanic alkalinity budget. Global Biogeochem. Cycles 25: 1–11. doi:10.1029/2010GB003859
12. Saderne, V., N. R. Geraldi, P. I. Macreadie, and others. 2019. Role of carbonate burial in Blue Carbon budgets. Nat. Commun. 10. doi:10.1038/s41467-019-08842-6
13. Macreadie, P. I., A. Anton, J. A. Raven, and others. 2019. The future of Blue Carbon science. Nat. Commun. 10: 1–13. doi:10.1038/s41467-019-11693-w

14. O'Mara, N. A., and J. P. Dunne. 2019. Hot Spots of Carbon and Alkalinity Cycling in the Coastal Oceans. Sci. Rep. 9: 1–8. doi:10.1038/s41598-019-41064-w
15. Saderne, V., Fusi, M., Thomson, T., Dunne, A., Mahmud, F., Roth, F., … Duarte, C. M. (2020). Total alkalinity production in a mangrove ecosystem reveals an overlooked Blue Carbon component. Limnology and Oceanography Letters. https://doi.org/10.1002/lol2.10170
16. Koch, M., G. Bowes, C. Ross, and X. H. Zhang. 2013. Climate change and ocean acidification effects on seagrasses and marine macroalgae. Glob. Chang. Biol. 19: 103–132. doi:10.1111/j.1365-2486.2012.02791.x
17. McLeod, E., G. L. Chmura, S. Bouillon, and others. 2011. A blueprint for blue carbon: Toward an improved understanding of the role of vegetated coastal habitats in sequestering CO2. Front. Ecol. Environ. 9: 552–560. doi:10.1890/110004
18. Bindoff, N.L., W.W.L. Cheung, J.G. Kairo, J. Arístegui, V.A. Guinder, R. Hallberg, N. Hilmi, N. Jiao, M.S. Karim, L. Levin, S. O'Donoghue, S.R. Purca Cuicapusa, B. Rinkevich, T. Suga, A. Tagliabue, and P. Williamson, 2019: Changing Ocean, Marine Ecosystems, and Dependent Communities. In: IPCC Special Report on the Ocean and Cryosphere in a Changing Climate [H.-O. Pörtner, D.C. Roberts, V. Masson-Delmotte, P. Zhai, M. Tignor, E. Poloczanska, K. Mintenbeck, A. Alegría, M. Nicolai, A. Okem, J. Petzold, B. Rama, N.M. Weyer (eds.)]. In press.
19. Thomas, S. 2014. Blue carbon: Knowledge gaps, critical issues, and novel approaches. Ecol. Econ. 107: 22–38. doi:10.1016/j.ecolecon.2014.07.028
20. Tramel, S. 2016. The Road Through Paris: Climate Change, Carbon, and the Political Dynamics of Convergence. Globalizations 13: 960–969. doi:10.1080/14747731.2016.1173376
21. Fourqurean, J. W., G. A. Kendrick, L. S. Collins, R. M. Chambers, and M. A. Vanderklift. 2012b. Carbon, nitrogen and phosphorus storage in subtropical seagrass meadows: Examples from Florida Bay and Shark Bay. Mar. Freshw. Res. 63: 967–983. doi:10.1071/MF12101
22. Van Dam, B. R., C. C. Lopes, P. Polsenaere, R. M. Price, A. Rutgersson, and J. W. Fourqurean. 2020. Water temperature control on CO2 flux and evaporation over a subtropical seagrass meadow revealed by atmospheric eddy covariance. Limnol. Oceanogr. 1–18. doi:10.1002/lno.11620
23. Millero, F.J., Hiscock, W., Huang, F., Roche, M. 2001. Seasonal Variation of the Carbonate System in Florida Bay. Bull. Mar. Sci. 68: 101–123
24. Zhang, J.-Z., and C. J. Fischer. 2014. Carbon Dynamics of Florida Bay: Spatiotemporal Patterns and Biological Control. Environ. Sci. Technol. 48: 9161–9169. doi:10.1021/es500510z
25. Oreska, M. P. J., K. J. McGlathery, L. R. Aoki, A. C. Berger, P. Berg, and L. Mullins. 2020. The greenhouse gas offset potential from seagrass restoration. Sci. Rep. 10: 1–15. doi:10.1038/s41598-020-64094-1
26. Walter, L.M., T. C. W. Ku, K. Muehlenbachs, W. P. Patterson, and L. Bonnell. 2007. Controls on the δ13C of dissolved inorganic carbon in marine pore waters: An integrated case study of isotope exchange during syndepositional recrystallization of biogenic carbonate sediments (South Florida Platform, USA). Deep. Res. Part II Top. Stud. Oceanogr. 54: 1163–1200. doi:10.1016/j.dsr2.2007.04.014
27. Hu, X., and D. J. Burdige. 2007. Enriched stable carbon isotopes in the pore waters of carbonate sediments dominated by seagrasses: Evidence for coupled carbonate dissolution and reprecipitation. Geochim. Cosmochim. Acta 71: 129–144. doi:10.1016/j.gca.2006.08.043
28. Chambers, R. M., Fourqurean, J. W., Macko, S. A., & Hoppenot, R. (2001). Biogeochemical effects of iron availability on primary producers in a shallow marine carbonate environment. *Limnology and Oceanography*, *46*(6), 1278–1286. https://doi.org/10.4319/lo.2001.46.6.1278
29. Holmer, M. and H. Hasler-Sheetal. 2014. Sulfide intrusion in seagrasses assessed by stable sulfur isotopes - a synthesis of current results. 1: 1–12. doi:10.3389/fmars.2014.00064
30. Hasler-Sheetal, H., and M. Holmer. 2015. Sulfide intrusion and detoxification in the seagrass zostera marina. PLoS One 10: 1–19. doi:10.1371/journal.pone.0129136
31. Eyre, B. D., D. Maher, J. M. Oakes, D. V. Erler, and T. M. Glasby. 2011. Differences in benthic metabolism, nutrient fluxes, and denitrification in Caulerpa taxifolia communities compared to uninvaded bare sediment and seagrass (Zostera capricorni) habitats. Limnol. Oceanogr. 56: 1737–1750. doi:10.4319/lo.2011.56.5.1737
32. Eyre, B. D., and A. J. P. Ferguson. 2002. Comparison of carbon production and decomposition, benthic nutrient fluxes and denitrification in seagrass, phytoplankton, benthic microalgae- and macroalgae-dominated warm-temperate Australian lagoons. Mar. Ecol. Prog. Ser. 229: 43–59. doi:10.3354/meps229043
33. Gardner, W. S., and M. J. McCarthy. 2009. Nitrogen dynamics at the sediment-water interface in shallow, subtropical Florida Bay: Why denitrification efficiency may decrease with increased eutrophication. Biogeochemistry 95: 185–198. doi:10.1007/s10533-009-9329-5
34. Eyre, B. D., I. R. Santos, and D. T. Maher. 2013. Seasonal, daily and diel N_2 effluxes in permeable carbonate sediments. Biogeosciences 10: 2601–2615. doi:10.5194/bg-10-2601-2013
35. Zeller MA, Van Dam BR, Lopes C and Kominoski JS. 2020. Carbonate-Associated Organic Matter Is a Detectable Dissolved Organic Matter Source in a Subtropical Seagrass Meadow. Front. Mar. Sci. 7:580284. doi: 10.3389/fmars.2020.580284
36. Long, M., P. Berg, and J. Falter. 2015. Seagrass metabolism across a productivity gradient using the eddy covariance, Eulerian control volume, and biomass addition techniques. J. Geophys. Res. Ocean. 120: 2676–2700. doi:10.1002/2014JC010441.

37. Frankovich, T. A., and J. C. Zieman. 1994. Total epiphyte and epiphytic carbonate production on Thalassia testudinum across Florida Bay. Bull. Mar. Sci. 54: 679–695.
38. Bosence, D. W. J. 1989. Biogenic Carbonate Production in Florida Bay. Bull. Mar. Sci. 44: 419–433.
39. Armitage, A. R., and J. W. Fourqurean. 2016. Carbon storage in seagrass soils: Long-term nutrient history exceeds the effects of near-term nutrient enrichment. Biogeosciences 13: 313–321. doi:10.5194/bg-13-313-2016
40. Gullström, M., L. D. Lyimo, M. Dahl, and others. 2018. Blue Carbon Storage in Tropical Seagrass Meadows Relates to Carbonate Stock Dynamics, Plant–Sediment Processes, and Landscape Context: Insights from the Western Indian Ocean. Ecosystems 21: 551–566. doi:10.1007/s10021-017-0170-8
41. Sanders, C. J., D. T. Maher, J. M. Smoak, and B. D. Eyre. 2019. Large variability in organic carbon and CaCO3 burial in seagrass meadows: A case study from three Australian estuaries. Mar. Ecol. Prog. Ser. 616: 211–218. doi:10.3354/meps12955
42. Stockman, K.W., R.N. Ginsburg, and E.A. Shinn. 1967. The production of lime mud by algae in south Florida. Journal of Sedimentary Petrology 37: 633-648.
43. Ginsburg, R.N. 1956. Environmental relationships of grain size and constituent particles in some south Florida carbonate sediments. American Association of Petroleum Geologists 40: 2384-2427.
44. Akhand, A., K. Watanabe, A. Chanda, and others. 2021. Lateral carbon fluxes and CO2 evasion from a subtropical mangrove-seagrass-coral continuum. Sci. Total Environ. 752: 1–14. doi:10.1016/j.scitotenv.2020.142190

Methods

Site description and sample collection

All collection of discrete samples was carried out in November 2019 at a well-characterized and shallow site (~1 m depth, 25°1.718'N, 80°40.736W) near Bob Allen Keys in central Florida Bay, one of the largest seagrass-dominated estuaries in the world. Sediments consist to 70-90% of carbonate minerals[21], mostly aragonite and high Mg-calcite[26], with relatively low iron content[28,45], and only trace amounts of silicate minerals[46]. The site is colonized by *Thalassia testudinum* (Turtle Grass) at a moderate density of ~5-25 % areal cover, while diverse calcareous green macroalgae are also present at <5% areal cover[47].

We sampled at 3 locations in close proximity within this seagrass meadow, representing regions of 1) high seagrass aboveground biomass (HD), 2) low seagrass density (LD), and 3) bare sediment (B). Quadruplicate 10 cm cores were collected for a continuous-flow incubation in which net sediment-water fluxes were directly measured, using cores that either included or excluded living seagrass biomass. This steady-state incubation does not represent net ecosystem metabolism because it was conducted in the dark. Rather, the intent was to create net conditions representative of night-time heterotrophy when denitrification is expected to be greatest[31], thereby providing a conservative estimate for the maximum anaerobic alkalinity that could be expected, across a realistic range in seagrass density. Separately, duplicate 30-50 cm sediment cores were collected at HD and LD sites for pore-water and solid-phase analysis.

Sediment and pore-water sampling and analysis

For solid-phase characterization, we collected 50 cm cores at both HD and LD sites, and sub-sampled at 5-cm intervals. Compaction was not apparent visibly, or in bulk density profiles. Sediment was freeze-dried, ground, and microwave-digested in a solution of 5 mL concentrated HNO_3 and 2 mL concentrated HCl, prior to trace-metal analysis by ICP-MS/MS[48]. Additional sediment was frozen, freeze-dried, and analyzed for $\delta^{13}C$ of the inorganic carbonate fraction ($\delta^{13}C_{PIC}$), or preserved with 25% $Zn(OAc)_2$ for analysis of Chromium Reducible Sulfur (CRS, a proxy for S^o and FeS_2), and acid volatile sulfide (AVS, a proxy for H_2S and FeS). The AVS and CRS fractions were extracted from the sediments as measured as in[49]. Duplicate acrylic cores of 25-35 cm length were also collected, and pore-water was sampled at 5 cm resolution using Rhizons (0.12 µm filtration) on the same day. Pore-water was preserved ($HgCl_2$ or $Zn(OAc)_2$) and analyzed for concentration and $\delta^{13}C$ of dissolved inorganic carbon ($\delta^{13}C_{DIC}$) and total sulfide concentration[50]. $\delta^{13}C$ measurements of DIC and $CaCO_3$ were carried via isotope ration monitoring mass spectrometry as described by[51] and[52], respectively.

Air-water CO_2 fluxes

Air-water CO_2 fluxes were continuously monitored by atmospheric EC, such that the flux footprint captured the spatial domain of sediment and pore-water sampling. CO_2 fluxes were calculated in EddyPro (Li-Cor Biosciences) at 30-minute intervals from continuous high-frequency (10 Hz) data, and these 30-minute fluxes were averaged to generate the daily or hourly fluxes presented in figure 1B&C. Detailed methods for these EC measurements and associated data screening procedures are identical to those applied previously[22].

Measured sediment-water flux

Quadruplicate cores of 10 cm deep, 6.4 cm diameter were collected at site B, and at two separate sub-sites for HD and LD, one set containing aboveground seagrass biomass, and the other omitting biomass. These cores were incubated under continuous flow with aerated site water at room temperature and in the dark. This setup prevented changes between net photosynthesis and respiration driven by light-to-dark transitions, a necessary step to ensure that calculated denitrification and DOC fluxes were representative of steady state conditions[53]. Net

sediment-water fluxes of N_2 (net denitrification) and DOC (Figure 1) were determined from the difference between each outflow and inflow of site reference water[53]. N_2 in effluent water was measured by membrane inlet mass spectrometry (MIMS), while DOC was measured on a OI Anaytical 1030D Total Organic Carbon Analyzer. By convention, positive fluxes represent a release from the sediment to the overlying water.

Modeled Sediment-water flux

Direct measurements of sediment-water fluxes were augmented by advective-diffusive modeling in PROFILE[54] for H_2S and DIC. We assumed no irrigation, and estimated bio-diffusivity in the upper 15 cm of sediment at 1 and 3 $cm^2\ hr^{-1}$ (0.00028 and 0.00083 $cm^2\ sec^{-1}$) at the LD and HD sites respectively, representing seagrass O_2 pumping into the rhizosphere. We arrived at these parameterizations through iterative calculation runs attempting to match model output DIC concentration profiles and vertical flux with measured DIC profiles and fluxes. Molecular diffusivity was calculated at in-situ temperature and salinity, using the 'marelac' package[55] in R. Boundary conditions at the top were set by the surface water concentration, and at the bottom of the model domain by a diffusive flux calculated from the gradient across the bottom two concentration measurements.

Budget Creation

Finally, we constructed a carbon and alkalinity budget, combining literature sediment accumulation rates[37,38] with our solid-phase results to estimate net accumulation of $CaCO_3$, and reduced sulfur and iron species. Using the stoichiometry outlined in Table 1, these burial rates were converted into net fluxes of DIC and TA, which were in turn used to calculate the CO_2 production or consumption due to each biogeochemical process. The ultimate goal of this exercise was to compare budgeted excess CO_2 with the excess CO_2 that would be required to sustain the CO_2 fluxes that were directly observed in this study.

Table 1. Selection of generalized biogeochemical reaction pathways affecting TA and DIC.

Process	**Generalized Reaction**	**Δ TA**	**Δ DIC**	**Inferred From**
Primary Production	$CO_2 + H_3PO_4 + HNO_3 \rightarrow OM + O_2$	**0***	**- 1**	O_2, Nutrient flux
Sulfate Reduction + Burial as 50% FeS_2 and 50% S^0	$4\,OM + 2SO_4^{2-} + 2H^+ \rightarrow 4CO_2 + 2H_2S$ + $0.5 \times [FeS + H_2S \rightarrow FeS_2 + H_2]$ $0.5 \times [O_2 + 2H^+ + H_2S \rightarrow S^o + 2H_2O]$	**+2** $1 + \frac{0+2}{2}$	**+1** $1 + \frac{0+0}{2}$	CRS
Fe Reduction	$OM + 2Fe_2O_3 + 8H^+ \rightarrow 2CO_2 + 4Fe^{2+}$	**+ 8**	**+ 2**	Fe – CRS
Canonical Denitrification	$OM + 0.8\,HNO_3 \rightarrow CO_2 + 0.4N_2 + NH_3 + H_3PO_4$	**+ 0.8**	**+ 1**	N_2 Flux
$CaCO_3$ Precipitation	$Ca^{2+} + 2HCO_3^- \rightarrow CaCO_3 + CO_2 + H_2O$	**- 2**	**- 1**	Range of Literature $CaCO_3$ Accumulation Rates

We assumed a range in literature carbonate accumulation rates[37,38] of 1.9 to 1042 g $m^{-2}\ yr^{-1}$, or 0.019 to 10.4 mol $CaCO_3\ m^{-2}\ yr^{-1}$. According to our solid-phase analysis, this sediment is 97.5% inorganic carbon (IC), 2.1% organic carbon (OC), 0.3% Chromium Reducible Sulfide (CRS; representing FeS_2 and S^0), and approximately 0.5% "free" Fe (calculated as the difference between CRS and total Fe). The net impact of production and burial of IC and OC on TA and DIC are shown in Table 1. The role of sulfate reduction is rather more complicated, as the sulfide produced by sulfate reduction (ΔTA:ΔDIC = 1:1) may or may not react with various phases of Fe, with various effects[57] on TA. Therefore, we take a simplifying approach of assuming that CRS burial occurs in equal proportions as FeS_2 (ΔTA = 0) and S^0 (ΔTA= 2), such that the net burial of reduced sulfide results in the production of TA and DIC in a ratio of 2:1 (Table 1). The net formation of "free" Fe produces TA and DIC in a ratio[57] of 8:2. Our modeling and experimental results demonstrate that N cycling is tightly internally recycled, such that the *net* rates are indistinguishable from zero, meaning that the impact of net denitrification on sediment TA release can be neglected from this model. Similarly, because NOx flux was balanced very closely by NH_4 flux (not shown in figures), we can assume that the net effect of net ecosystem production on TA was small. These molar equivalents were combined with literature sediment accumulation rates (SAR) to estimate the change in water-column TA and DIC due to each of the above-mentioned processes (IC burial, OC burial, net SO_4 reduction [CRS], and Fe reduction).

We calculated the change in surface water CO_2 concentration ($\frac{\Delta CO_2}{CO_2}$) for each process using the above TA and DIC anomalies (X and Y; Table 1) and buffer factors for TA (γ_{TA}) and DIC (γ_{DIC}): $\frac{\Delta CO_2}{CO_2} = \frac{SAR \times X}{\gamma_{DIC}} + \frac{SAR \times Y}{\gamma_{TA}}$, as in (Egleston et al., 2010). Subsequently, the CO_2 concentration (μmol kg^{-1}) resulting from this $\frac{\Delta CO_2}{CO_2}$, using the 'seacarb' package[58] in RStudio. Initial conditions were set according to direct measurements in the water column

(TA: 2596 µmol kg^{-1}, DIC: 2295 µmol kg^{-1}, Sal: 38, Temp: 26 ºC). The Excess CO_2 (µmol kg^{-1}) shown in Figure 4 is the difference between initial CO_2 and the CO_2 concentration after sediment TA/DIC exchange. Water currents at this site are very minor[22], allowing us to exclude lateral exchanges from this simple model. However, an important implication of this model is that any net TA and DIC production/consumption is compensated by import/export with the coastal ocean, albeit over longer time scales.

Methods References

45. Ruiz-Halpern, S., S. A. Macko, and J. W. Fourqurean. 2008. The effects of manipulation of sedimentary iron and organic matter on sediment biogeochemistry and seagrasses in a subtropical carbonate environment. Biogeochemistry 87: 113–126. doi:10.1007/s10533-007-9162-7
46. Ku, T. C. W., L. M. Walter, M. L. Coleman, R. E. Blake, and A. M. Martini. 1999. Coupling between sulfur recycling and syndepositional carbonate dissolution: Evidence from oxygen and sulfur isotope composition of pore water sulfate, South Florida Platform, U.S.A. Geochim. Cosmochim. Acta 63: 2529–2546. doi:10.1016/S0016-7037(99)00115-5
47. Zieman, J. C., J. W. Fourqurean, and R. L. Iverson. 1989. Distribution, Abundance and Productivity of Seagrasses and Macroalgae in Florida Bay. Bull. Mar. Sci. 44: 292–311
48. Zimmermann, T., von der Au, M., Reese, A., Klein, O., Hildebrandt, L., & Pröfrock, D. (2020). Substituting HF by HBF 4 – an optimized digestion method for multi-elemental sediment analysis via ICP-MS/MS. *Analytical Methods*, *12*(30), 3778–3787. https://doi.org/10.1039/d0ay01049a
49. Seibert S.L., Böttcher M.E., Schubert F., Pollmann T., Giani L., Tsukamoto S., Frechen M., Freund H., Waska H., Simon H., Holt T., Greskowiak J., Massmann G. (2019) Iron sulfide formation in young and rapidly-deposited permeable sands at the land-sea transition zone. Sci. Tot. Env. 649, 264-283. https://doi.org/10.1016/j.scitotenv.2018.08.278
50. Cline, J. D. 1969. Spectrophotometric determination of hydrogen sulfide in natural waters. Limnol. Oceanogr. 14, 454–458
51. Winde V., Böttcher M.E., Escher P., Böning P., Beck M., Liebezeit G., Schneider B. 2014. Tidal and spatial variations of DI^{13}C and aquatic chemistry in a temperate tidal basin during winter time. J. Mar. Sys. 129, 394-402. https://doi.org/10.1016/j.jmarsys.2013.08.005
52. Böttcher M.E., Neubert N., Escher P., von Allmen K., Samankassou E., Nägler, T.F. 2018. Multi-isotope (Ba, C, O) partitioning during experimental carbonatization of a hyperalkaline solution. CdE - Geochemistry, 78, 241-247. https://doi.org/10.1016/j.chemer.2018.01.001
53. Smyth, A.R., Thompson, S.P., Siporin, K.N. et al. 2013. Assessing Nitrogen Dynamics Throughout the Estuarine Landscape. Estuaries and Coasts 36, 44–55. http://doi.org/10.1007/s12237-012-9554-3
54. Berg, P., Nils, R., Rysgaard, S. 1998. Interpretation of measured concentration profiles in sediment pore water, Limnology and Oceanography, 7, doi: 10.4319/lo.1998.43.7.1500
55. Soetaert, K., Petzoldt, T., and Meysman, F. 2016. Marelac: A tool for aquatic sciences (R package), available at: https://cran.r-project. org/web/packages/marelac/marelac.pdf.
56. Egleston, E. S., Sabine, C. L., & Morel, F. M. M. (2010). Revelle revisited: Buffer factors that quantify the response of ocean chemistry to changes in DIC and alkalinity. Global Biogeochemical Cycles, 24(1), 1–9. https://doi.org/10.1029/2008GB003407
57. Soetaert, K., Hofmann, A. F., Middelburg, J. J., Meysman, F. J. R., & Greenwood, J. (2007). The effect of biogeochemical processes on pH. Marine Chemistry, 106(1-2 SPEC. ISS.), 380–401. https://doi.org/10.1016/j.marchem.2007.06.008
58. Gattuso, J.-P., Epitalon, J.-M., Lavigne, H., Orr, J., Gentili, B., Hofmann, A., Proye, A., Soetaert, K., Rae, J., 2016. Seacarb: Seawater Carbonate Chemistry. http://CRAN.R- project.org/package=seacarb

Acknowledgements

We thank Peter Berg, Joey Crosswell and John Kominoski for the productive discussions. Sara Wilson, Iris Schmiedinger, Bettina Rust, and Stephen Richardson provided valuable assistance in the field and lab. This research was supported by institutional funding through HZG, and grants and funds from the German Academic Exchange Service (DAAD grant #57429828), the German Federal Ministry of Education and Research (BMBF), the U.S. National Science Foundation through the Florida Coastal Everglades Long-Term Ecological Research program (Grant No. DEB-1832229), and the National Institute of Food and Agriculture (FLA-TRC-005764). This is contribution #x from the Coastlines and Oceans Division of the Institute of Environment at Florida International University.

Author Contributions

The eddy covariance platform used during this study was conceived of by JWF and BRV, and constructed and operated by CL. The Fall 2019 study was conceived by BRV, AS, CL, MAZ, MEB, JWF and CLO, with field work conducted by BRV, AS, CL, and MAZ. AS carried out the laboratory incubation experiment, while remaining analytical work was conducted by BRV, MAZ, CL, AS, MEB, CLO, and TZ. This manuscript was written by BRV with significant contributions from all other authors.

Figures

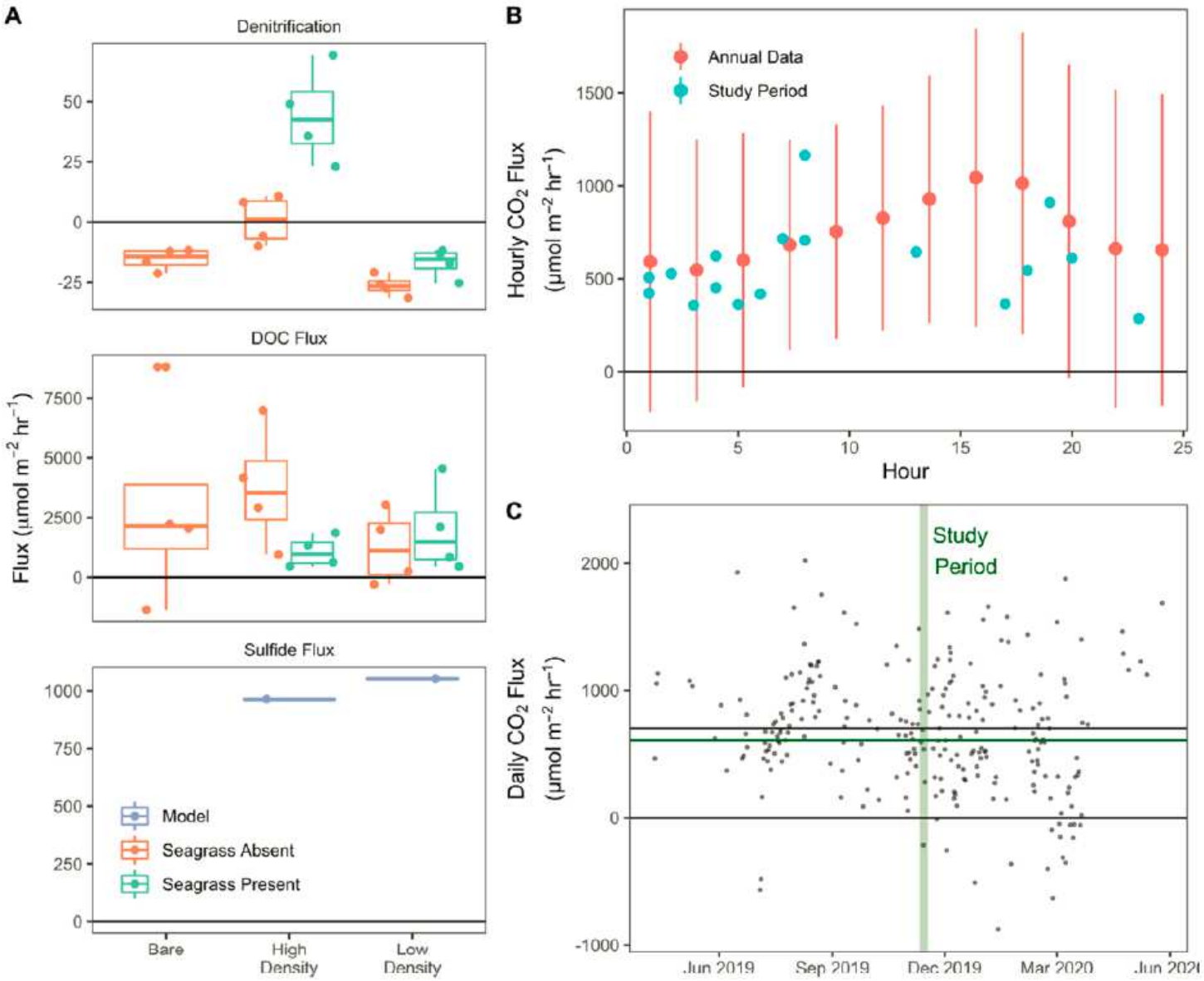

Figure 1

Boxplots showing average N2 flux (denitrification), DOC fluxes, and sulfide fluxes (A). Hourly and daily climatological mean CO2 fluxes, from direct EC measurements in the year surrounding the study period (B,C). In (C), the timeframe of the study period is highlighted in green, while mean CO2 fluxes from the study period and annually are shown as the green and black horizontal lines, respectively. By convention, release from sediments or water are reported as positive fluxes. All error bars represent x̄ ± standard deviation.

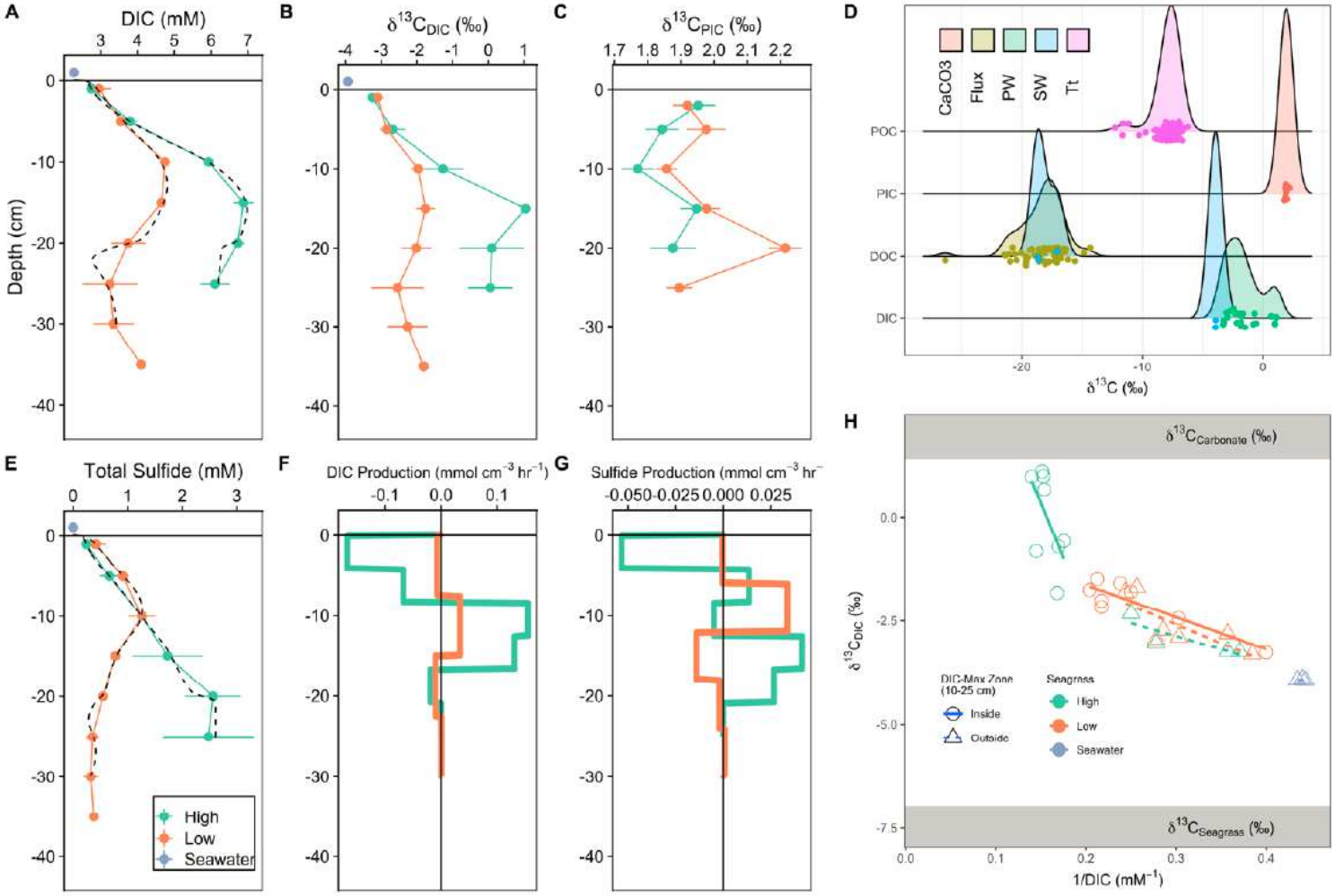

Figure 2

Vertical profiles of pore-water DIC, δ13CDIC, and δ13CPIC (A-C). Carbon isotopic signatures for selected pools (D). Total dissolved sulfide (E), and modeled production rates for DIC and total Sulfide (F, G). 'Keeling Plot' of pore-water δ13CDIC (H). Model output pore-water concentrations are shown in the black dotted lines in figures A-B (each core was modeled individually).

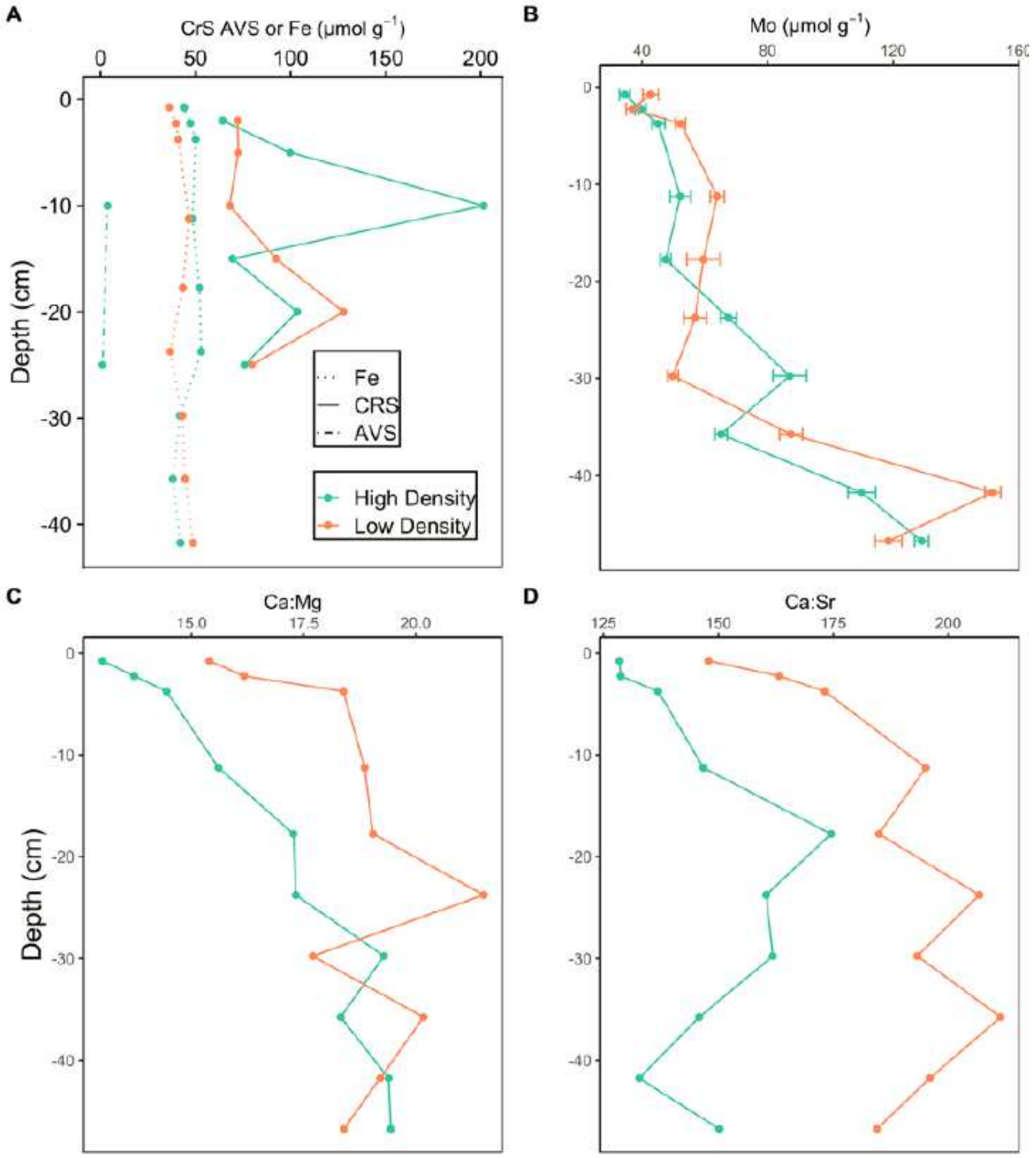

Figure 3

Solid-phase total Fe, Chromium Reducible Sulfur (CRS) and acid-volatile sulfide (AVS) (A), total Mo (B), and molar ratios of Ca:Mg and Ca:Sr (C,D).

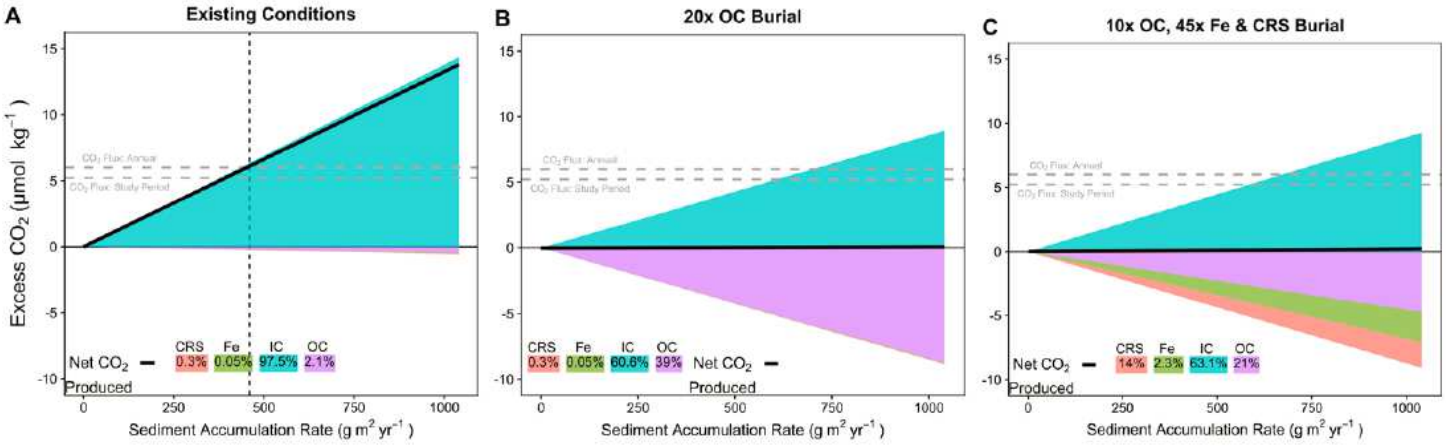

Figure 4

Modeled Excess CO2, across a range in literature sediment accumulation rates. The bottom subplot is a magnification of the terms constituting net CO2 uptake (burial of OC, reduced S and Fe). In figure (A) sediment fractions of CRS, Fe, IC, and OC were set according to direct measurements from this study. In figure (B), the OC fraction was artificially increased until Excess CO2 remained at 0 across the range in sediment accumulation, such that CO2 released by calcification was offset by CO2 consumed by OC burial, Fe and SO4 reduction. In figure (C), net CO2 balance was achieved by increasing OC, Fe, and CRS fractions by factors of 10, 45, and 45, respectively.